Engineering Structures 86 (2015) 168–181

Contents lists available at ScienceDirect

Engineering Structures

journal homepage: www.elsevier.com/locate/engstruct

Numerical modeling of reinforced concrete beams repaired and strengthened with SFRC

Gonzalo Ruano [a,b,*], Facundo Isla [a,b], Domingo Sfer [a], Bibiana Luccioni [a,b]

[a] Structures Institute, National University of Tucumán, Av. Independencia 1800, 4000 S.M. de Tucumán, Argentina[1]
[b] CONICET, Av. Rivadavia 1917, Bs As, Argentina

ARTICLE INFO

Article history:
Received 6 September 2013
Revised 20 November 2014
Accepted 15 December 2014
Available online 19 January 2015

Keywords:
Fiber reinforced concrete
Repairing
Strengthening
Shear
Reinforced concrete

ABSTRACT

Improved tensile properties of steel fiber reinforced concrete (SFRC) make it suitable for repairing and strengthening of reinforced concrete elements. The use of this material as repairing or strengthening material has increased during the last years motivating the development of numerical tools for the design of this type of intervention technique.

The numerical simulation of the mechanical behavior of a series of reinforced concrete beams which includes strengthened and repaired beams with high performance self compacting SFRC tested under shear is presented in this paper. SFRC is considered as a composite material composed of concrete matrix and fibers and a simple homogenization approach based on modified mixture theory is used to model its mechanical behavior. An evolutionary algorithm is proposed in order to simulate the whole process of testing, repairing and retesting the beams.

The numerical simulations can accurately reproduce flexure characterization tests and predict the bearing capacity of the repaired and strengthened beams tested under shear. Furthermore, other repairing/strengthening options are numerically studied. The numerical results could be useful to improve the design of this kind of intervention techniques.

1. Introduction

The reinforced concrete (RC) structures repairing or strengthening technique using fiber reinforced concrete (FRC) avoids some of the problems that other systems present like the brittle failure of the interface repairing or strengthening layer/concrete. Compared with fiber reinforced polymers, fiber reinforced cement composites present higher resistance against high temperature and ultraviolet radiation, longer term durability and, fundamentally, more compatibility with the substrate [1]. Moreover, the use of fibers in the repairing or strengthening concrete layer helps controlling shrinkage cracking.

The use of FRC for repairing or strengthening purposes of different types of concrete and RC elements like beams, columns, panels, joints, slabs and pavements is increasing nowadays and has been extensively investigated during the last years. Different types of cement based materials for the matrix like normal strength, high strength concrete or self consolidating concrete, were used and compared. Moreover different types, sizes and shapes of fibers were used.

A brief review on the principal fields of application of SFRC as strengthening and repairing material and the research work done in this area are presented in the following paragraphs.

The use of slurry infiltrated mat concrete (SIMCOM) for repair and rehabilitation of RC beams and columns was studied by Naaman et al. [2]. They concluded that SIMCOM can successfully interact with RC elements substantially increasing flexural strength and energy absorption capacity.

The flexure behavior of beams repaired with a bottom concrete layer of self compacting concrete and self compacting FRC was experimentally studied by Mesbah et al. [3]. The use of self compacting concrete has shown to be a good option to facilitate the pouring.

The use of ultra-high strength steel fiber-reinforced concrete (UFC) jacketing for the strengthening of internal nodes of RC frames was proposed by Wang and Lee [4]. They showed that the use of UFC leaded to an increase of ductility and the formation of plastic hinges in the beams.

A new material called ultra-high performance cement-based fiber composite (CARDIFRC) was presented by Farhat et al. [5]. It is an ultra high performance composite reinforced with 8% in

* Corresponding author. Tel.: +54 381 4364087.
E-mail address: gonzalo.ruano@gmail.com (G. Ruano).
[1] *URL:* http://www.herrera.unt.edu.ar/iest

http://dx.doi.org/10.1016/j.engstruct.2014.12.030
0141-0296/

Nomenclature

$(\alpha_i)_m$	set of internal variables for the mth component
A_{klij}	stress mapping fourth order tensor
γ	parameter to control the shape of yield function in the octahedral plane
δ_{im}	Kronecker delta
E	Young modulus
E_{ij}	elasticity modulus in ith direction
ε_{ij}	total strain tensor for the composite
$(\varepsilon_{ij})_n$	strain tensor for the nth component
ε^e_{ij}	elastic strain tensor
ε^p_{ij}	plastic strain tensor
ε^s_{ij}	slipping strain tensor
F	yield function
f	equivalent stress
$\overline{F}$	fibers elastic limit threshold defined in the fictitious isotropic space
$\bar{f}$	equivalent stress in the fictitious isotropic space
F_L	flexure strength
F^{ps}	fibers elastic limit threshold
G	plastic potential function
G_c	crushing energy
g_c	maximum energy densities dissipated in uniaxial compression
G_f	fracture energy
g_f	maximum energy densities dissipated in uniaxial tension
H	heaviside function
K	yield threshold
$\overline{K}$	hardening function in the fictitious isotropic space
k_{Fi}	fiber content in ith direction
k_m	volumetric fraction corresponding to mth component
κ^p_{comp}	plastic hardening variable value for the concrete peak compression stress
κ^p	plastic damage variable or isotropic plastic hardening variable
$\dot{\lambda}$	plastic consistency parameter
l_c	external parameter depending on the finite element mesh
r	normalized ramp function defined in Eq. (9)
R^{0p}	compression/tension elastic limit ratio
R^{bc}	compression equibiaxial/uniaxial ratio
σ_c	yield threshold evolution in uniaxial compression
σ_i	yield stress in ith direction
σ_{ic}	principal concrete stresses
σ_{ij}	stress tensors in actual orthotropic space
$(\sigma_{ij})_m$	stress tensor for the mth component
σ_m	compression strength
$\bar{\sigma}_{mn}$	elastic threshold in the actual orthotropic space
σ_t	yield threshold evolution in uniaxial tension
σ_{uc}	uniaxial compression strength
σ_{utx}	uniaxial tensile slip strength in axial direction
σ_{stx}	uniaxial tensile slipping threshold in axial direction
σ_y	yield stress
σ_{yc}	uniaxial compression yield threshold
$\bar{\tau}$	elastic threshold in the fictitious isotropic space
τ_{kl}	stress tensors in fictitious isotropic space
ν	Poisson ratio
ν_{ij}	Poisson ratio in ith direction
$\Psi(\varepsilon_{ij}, \alpha_i)$	composite free energy density per volume unity
$\Psi_m(\varepsilon_{ij}, (\alpha_i)_m)$	free energy density per volume unity of each m-component
$(\cdot)_c$	subscript for concrete
$(\cdot)_{Fi}$	subscript for ith fiber orientation
$(\cdot)^{ps}$	superscript for inelastic (plastic/slip) in fibers

volume of short fibers. They used this material for the reinforcement of under reinforced concrete beams under flexure and over reinforced concrete beams under shear. In all strengthening setups the strength of the beams was increased with the reinforcement.

Experimental results of two actual scale bridge piles repaired with high performance fiber reinforced concrete (HPFRC) were presented by Massicotte and Boucher [6]. The strengthened pile presented greater load bearing capacity, increasing with load cycles, and also greater ductility.

An ultra high performance fiber reinforced concrete (UHPFRC) was used by Brühwiler and Denarié [7] to restore RC structures that have suffered environment attacks and surface mechanical actions. They showed some applications already done in bridge decks, highways protection barriers, bridge piles and industrial floors.

The efficiency of high performance fiber-reinforced micro-concrete as a repair material when applied on concrete beams was evaluated by Skazlic et al. [8] and they concluded that the use of this material for repairing purposes has both economical and technical advantages.

The behavior of rectangular concrete plates used as industrial pavements repaired with FRC was studied by Boscato and Russo [9]. They achieved excellent adherence between the materials and increase of the first crack load and the collapse load.

A self compacting FRC jacketing was used by Martinola et al. [10] to strengthen and repair RC beams predominantly subjected to flexion. They obtained good adherence between the jacketing and the beams and the flexural strength and stiffness were increased.

An overview of the different possible applications of HPFRC for strengthening or repairing existing RC structures was presented by Maringoni et al. [11] and the benefits in terms of bearing capacity, stiffness and durability were discussed.

RC beams were repaired by Iskhakov et al. [12] replacing the compression zone concrete by steel fiber reinforced high strength concrete (SFHSC) and creating two layers beams. The addition of steel fibers increased ultimate deformations and provided supplementary energy dissipation to the structure.

A patch repair method that uses high performance fiber reinforced cement composites to repair RC members damaged by chloride attack was presented by Iskhakov et al. [12]. Strength could be recovered if the amount of corrosion was less than 10%.

The numerical simulation of the mechanical behavior of a series of reinforced concrete beams which includes strengthened and repaired beams with high performance self compacting SFRC tested under shear is presented in this paper. First some numerical models for SFRC developed by other authors are briefly reviewed. Then the experimental program and the main properties of the RC beams analyzed are presented. Next, the constitutive model used is described and the algorithm developed to simulate the behavior of repaired beams is presented. The comparison between numerical and experimental results is used to validate the numerical model developed. Finally, the paper is completed with the numerical simulation of non tested alternatives. Useful conclusions for the design of shear strengthening/repairing of RC beams with SFRC are obtained.

2. Numerical models for SFRC. Brief review

Although some experimental works related to the use of fiber reinforced composites with cement like matrix for the repairing or strengthening of RC structures have been published, practical tools for the design of this type of intervention techniques are still in development. The prediction of the response of repaired or strengthened structures usually requires the numerical simulation of the resulting composite structures.

While concrete and RC behavior under multi-axial loads has been well studied, documented and modeled by several researchers, several differences between the constitutive models proposed for FRC in the existing codes can be found [13].

Constitutive models for SFRC can be classified in macro-models, meso-models and micro models according to the scale in which they are defined.

In macro-models the composite material is represented as a unique material with average properties. These types of model are usually based on a phenomenological approach in which the constitutive laws are obtained from laboratory tests. In general, models originally developed for plain concrete are modified to simulate the behavior of SFRC. These models are based on different approaches for the continuum like hypoelastic models [14] microplane models [15], smeared crack models [16], hardening elastoplastic models [17], elastoplastic Willam-Warnke models [18], damage models [19,20] or non linear models calibrated with experimental results from tension and compression tests [21].

The main task in this type of approach is the definition of the tensile behavior of SFRC that can be measured in direct tension tests or indirectly obtained through an inverse analysis from bending tests results [22]. The advantage of this phenomenological approach is the use of material information at the relevant scale for the analysis of the structure [23]. The main drawback is the need of extensive and costly experimental tests [23]. Since meso-mechanical behavior is not explicitly modeled, fiber volume fraction, aspect ratio, type, distribution and orientation cannot be taken into account. These data are relevant for SFRC concrete behavior and new experimental results should be obtained every time any of them is changed.

Many of these problems can be avoided with meso-mechanical derived models in which constitutive materials, concrete and fibers, and sometimes fiber/matrix interface are explicitly taken into account or with micro-mechanical models in which the components of concrete: mortar and aggregates are additionally considered. The development of constitutive models relating the meso-structural or micro-structural parameters to the mechanical behavior of fiber composites is also motivated by the possibility of designing the material for each application and predicting the behavior of the designed material [24].

Constitutive relations meso-mechanically or micro-mechanically derived involve two major steps: (1) derivation of crack bridging force for a single fiber in terms of meso-parameters and (2) derivation of the composite behavior for a given fiber distribution [25]. Models differ in the way in which these two steps are developed and combined.

The derivation of the crack bridging forces can be done from experimental pull out tests or meso-mechanically derived [26–30].

Some meso-mechanical approaches explicitly model the fibers using different types of discrete elements [31,32]. Some of these models also use a multi-scale approach [33,34] to represent the composite behavior at the macro-scale.

Alternatively, instead of modeling the fibers Radtke et al. [35] consider the fiber reactions that are applied to the matrix nodes including a fix radius surrounding the fibers ends.

Other authors use simpler homogenization models like Mori Tanaka [23] or classic mixture theory [36,29,37] to model the composite behavior as a function of the fiber volume fraction, orientation and geometric and mechanical properties without the need of explicitly modeling them. Brighenti et al. [38] compare a discontinuous-like finite element (FE) approach and a lattice model for FRC. They show that the lattice model gives a detailed description of the fracture pattern, while the discontinuous FE approach mainly gives only global information.

A simple homogenization approach for SFRC based on a modified mixture theory was proposed by the authors in a previous paper [39]. SFRC is considered as a composite material composed by concrete matrix which is modeled with an elastoplastic model [40,41] and steel fibers considered as orthotropic elastoplastic inclusions that can debond and slip from the matrix. Constitutive equations of fibers are modified using the approach proposed by Luccioni and López [42] in order to include this inelastic phenomenon without explicitly modeling the interface. The model requires concrete properties, fibers material, geometry, distribution and orientation as input data. The fibers bond–slip behavior is obtained from pull out tests.

This model is used in the present paper to simulate the mechanical response of RC beams strengthened and repaired with SFRC tested under shear.

3. Experimental program

The main objective of the experimental program was the evaluation of the SFRC performance as shear repairing/strengthening system for RC beams, specially the contribution of the steel fibers to the behavior of the repaired/strengthened beams [43]. For this purpose, RC beams were designed according to CIRSOC 201-2005 [44] standard which has the same requirements as ACI-318-2005 [45] standard to present shear failure.

The program consisted of a total of 14 RC beams with stirrups casted together. The dimensions and reinforcement of the RC beams tested are shown in Fig. 1(a) while the main characteristics of the different specimens are summarized in Table 1. Some of the beams were damaged, repaired with SFRC and retested. These beams are called repaired beams in Table 1. The rest of the beams were initially strengthened with SFRC and tested. These beams are called strengthened beams in Table 1.

The beams were repaired/strengthened with a high performance self compacting SFRC jacketing. See Fig. 1(b). To study the effect of fibers addition, three types of repairing/strengthening material were used, plain concrete and SFRC with two different steel fibers dosages, 30 kg/m^3 and 60 kg/m^3. According to previous experimental tests 60 kg/m^3 was the maximum fiber content compatible with SFRC workability and casting of the SFRC jacketing. 30 kg/m^3 was chosen as an intermediate value between 60 kg/m^3 and 0 kg/m^3 corresponding to plain concrete.

In all cases, the jacketing thickness was 30 mm. 50 mm length and 1 mm diameter hooked end steel fibers with yield strength of 860 MPa (normal strength fibers) were used for SFRC jacketing. The average mechanical properties of concrete used for the beams and for the different types of jacketing and the properties of the steel rebars used in RC beams are presented in Tables 2 and 3 respectively. Concrete properties were obtained from compression tests of cylindrical specimens and flexure tests of notched beams ($150 \times 150 \times 600$ mm) performed at the same age of the beams' tests, more than 28 days in all cases. Both strength and elasticity modulus of longitudinal steel bars were obtained from tension tests while for stirrups and hangers only the bars' strength was measured and a typical value was considered for the elasticity modulus.

The beams were tested under asymmetric flexure with an INSTRON 8504 press; see Fig. 1(c). The displacement of the load appli-

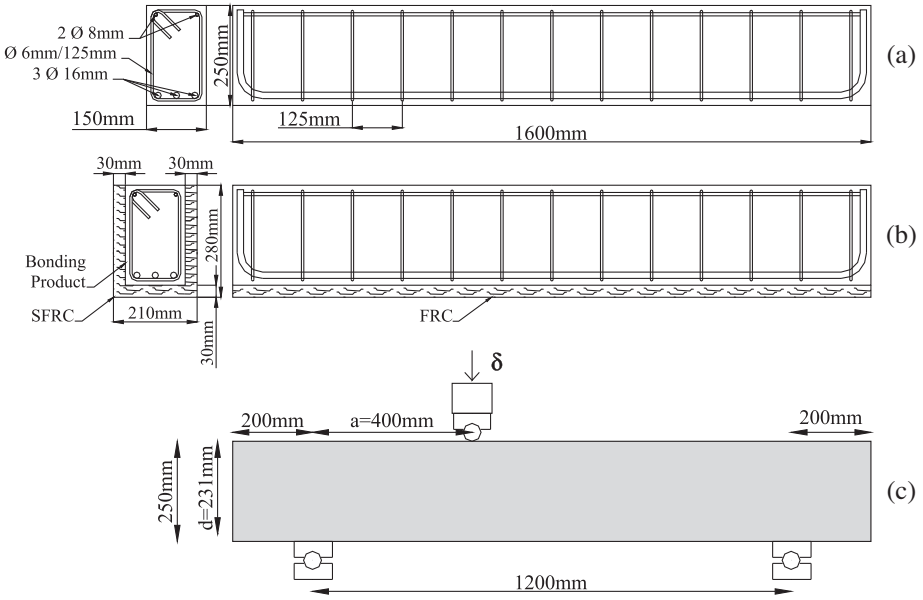

Fig. 1. (a) RC beam. (b) Repaired/strengthened beam. (c) Test setup.

Table 1
Beams tested.

Beam	Treatment	Fiber content (kg/m^3)
1; 2	Str.	–
4; 5; 6	Rep.	–
7; 8	Str.	30
10; 11; 12	Rep.	30
13; 14	Str.	60
16; 17	Rep.	60

Str.: strengthened, Rep.: repaired.

Table 2
Plain concrete average properties.

Materials Properties	Beams	Jacketing (concrete matrix for SFRC)
Compression strength σ_m (Pa)	26.3	95.3
Young modulus E (GPa)	24.0	41.5
Flexure strength F_L (kN)	12.2	16.4

Table 3
Steel rebar average properties.

Steel	Yield stress σ_y (MPa)	Young modulus E (GPa)
Long. bars	489.9	191.2
Stirrups	520.1	200.0
Hangers	452.5	200.0

cation point was recorded. The beams were first tested under load control and then, with displacement control going through the peak load and getting part of the descending branch of the load–deflection curve. Finally, they were unloaded in a controlled way. An increasing load 0.167 kN/s to reach 30 kN was first applied; then, the test was continued with a displacement rate of 0.5 mm/min.

A displacement criterion was used to define the extent of damage previous to the repairing of beams. Most of the RC beams were tested up to a displacement of 12mm shift. However, some of them showed a very pronounced softening after the maximum load and the tests were stopped when the load decreased to 70% of the maximum load, before that displacement (12 mm) was reached. The strengthened/repaired beams were tested up to a deflection of 14 mm.

Experimental results show that repair or strengthening with SFRC jacketing improves the RC beams behavior under shear. The principal effect of fibers addition to the jacketing was preventing debonding from the RC beam [43].

The particular objective of strengthening was the increase of load bearing capacity. Statistically, the RC beams strengthened with SFRC increased their shear strength while for the case of beams strengthened with plain concrete no strength increase was found [43]. In conclusion, the fiber reinforced concrete jacketing looks like an efficient method for shear strengthening of RC beams [43].

The particular objective of repairing was the restitution of the original load bearing capacity. Statistically, the beams repaired with SFRC presented greater strength than the original beams when they were not excessively damaged in previous test. Concluding, SFRC jacketing with at least 30 kg/m^3 of fibers seems to be an efficient shear repairing method for RC beams but the percentage of strength recovery depends on the severity of previous damage [43].

4. Constitutive models

SFRC can be regarded as composite material consisting of a brittle concrete matrix plus short disperses fibers. One of the simplest ways of modeling composites behavior is mixture theory [46–48]. This paper employs modified mixture theory for orthotropic materials to simulate SFRC behavior taking into account the concrete and fibers contribution. Particularly, the anisotropic behavior of fibers and their slipping are modeled in a simplified way [39].

Tensor notation is used in all the following equations, scalars have no index, vectors are identified with one index, second order tensors like strain and stress tensors are identified with two sub index while fourth order tensor like stiffness tensors are identified with four sub index.

4.1. Composite material

The classic theory of mixtures is based on the following assumptions [46–48],

(1) The set of component substances is present in each infinitesimal volume of the composite.

(2) Each component contributes to the behavior of the composite in proportion to its volumetric participation.
(3) The volume occupied by each component is lesser than the volume occupied by the composite.
(4) All the components have the same strain (compatibility condition).

For small strains, and n-component composite materials this last assumption is written

$$\varepsilon_{ij} = (\varepsilon_{ij})_1 = (\varepsilon_{ij})_2 = \cdots = (\varepsilon_{ij})_n \tag{1}$$

where ε_{ij} and $(\varepsilon_{ij})_n$ are the strain tensors for the composite and the nth component.

On the other hand, the composite free energy density can be written

$$\Psi(\varepsilon_{ij}, \alpha_i) = \sum_{m=1}^{n} k_m \Psi_m(\varepsilon_{ij}, (\alpha_i)_m) \tag{2}$$

where $\Psi_m(\varepsilon_{ij}, (\alpha_i)_m)$ is the free energy density per volume unity of each m-component, $k_m = dV_m/dV$ is the corresponding volumetric ratio and $(\alpha_i)_m$ is a set of internal variables.

The composite secant constitutive equation can be obtained from Coleman relations that guarantee the fulfillment of Clasius-Duhem inequality [49]:

$$\sigma_{ij} = \frac{\partial \Psi(\varepsilon_{kl}, \alpha_k)}{\partial \varepsilon_{ij}} = \sum_{m=1}^{n} k_m \frac{\partial \Psi_m(\varepsilon_{kl}, (\alpha_k)_m)}{\partial \varepsilon_{ij}} = \sum_{m=1}^{n} k_m (\sigma_{ij})_m \tag{3}$$

where each m-component stress tensor $(\sigma_{ij})_m$ is obtained from the constitutive equations respectively.

SFRC is considered as a composite formed by a concrete matrix identified with c subscript and fibers oriented in three orthogonal directions x, y and z and identified with F_x, F_y and F_z subscript respectively. The fiber/matrix interface is not explicitly considered.

Compatibility condition Eq. (1) is written as

$$(\varepsilon_{ij})_{SFRC} = (\varepsilon_{ij})_c = (\varepsilon_{ij})_{F_x} = (\varepsilon_{ij})_{F_y} = (\varepsilon_{ij})_{F_z} \tag{4}$$

It should be noted that Eq. (4) is a strong restrain. It is well known that fiber slipping over the matrix plays an important role in SFRC behavior, especially in post-cracking stage. Therefore, Eq. (4) is retained but the fibers constitutive model is modified to take into account slipping without explicitly modeling the interface. The fibers total strain is supposed to represent both the fibers and the interface strains and to be formed by an elastic strain ε^e_{ij}, a plastic strain ε^p_{ij} and a slipping strain ε^s_{ij}

$$\begin{aligned}
(\varepsilon_{ij})_{F_x} &= \left(\varepsilon^e_{ij}\right)_{F_x} + \underbrace{\left(\varepsilon^p_{ij}\right)_{F_x} + \left(\varepsilon^s_{ij}\right)_{F_x}}_{\left(\varepsilon^{ps}_{ij}\right)_{F_x}} \\
(\varepsilon_{ij})_{F_y} &= \left(\varepsilon^e_{ij}\right)_{F_y} + \underbrace{\left(\varepsilon^p_{ij}\right)_{F_y} + \left(\varepsilon^s_{ij}\right)_{F_y}}_{\left(\varepsilon^{ps}_{ij}\right)_{F_y}} \\
(\varepsilon_{ij})_{F_z} &= \left(\varepsilon^e_{ij}\right)_{F_z} + \underbrace{\left(\varepsilon^p_{ij}\right)_{F_z} + \left(\varepsilon^s_{ij}\right)_{F_z}}_{\left(\varepsilon^{ps}_{ij}\right)_{F_z}}
\end{aligned} \tag{5}$$

Strictly, only the first two terms (elastic and plastic) take place in fibers, the third term corresponds to inelastic fiber–matrix relative displacement that takes place at the interface. As a result of Eqs. (4) and (5), the strain in the fibers is not actually equal to that in the matrix. The last two terms in each equation constitute the inelastic strain ε^{ps}_{ij} that takes place at the set of fiber and fiber/matrix interface.

4.2. Concrete constitutive model

A modified plastic damage model is used for concrete [41]. The plastic behavior is obtained as a generalization of classical theory of plasticity especially appropriate for geomaterials. The elastic behavior limit is defined through a yield function,

$$F((\sigma_{ij})_c; (\kappa^p)_c) = f((\sigma_{ij})_c) - K((\sigma_{ij})_c; (\kappa^p)_c) \leqslant 0 \tag{6}$$

where $f((\sigma_{ij})_c)$ is the equivalent stress. A modified Lubliner-Oller yielding criterion is used in this paper [41]. $K((\sigma_{ij})_c; (\kappa^p)_c)$ is the yield threshold and $(\kappa^p)_c$ is the plastic damage variable or isotropic plastic hardening variable.

The following flaw rule is defined for the plastic strains.

$$\left(\dot{\varepsilon}^p_{ij}\right)_c = \dot{\lambda} \frac{\partial G((\sigma_{mn})_c; (\kappa^p)_c)}{\partial (\sigma_{ij})_c} \tag{7}$$

where $\dot{\lambda}$ is the plastic consistency parameter and G is the plastic potential function. Lubliner-Oller [50] function is used for G.

The plastic hardening variable κ^p is obtained normalizing energy plastically dissipated to unity and varies between 0 for the virgin material and 1 when the material has dissipated all the available energy. The evolution law for the plastic hardening variable takes into account the differentiated behavior in tension and compression and properly simulates energy dissipation for triaxial compression processes [51],

$$(\dot{\kappa^p})_c = \left[\frac{r}{g^*_f} + \frac{(1-r)}{g^*_c}\right] (\sigma_{ij})_c (\dot{\varepsilon}^p_{ij})_c \tag{8}$$

where

$$r = \frac{\sum_{i=1}^{3} |\sigma_{ic}|}{\sum_{i=1}^{3} |\sigma_{ic}|} \geq 0 \quad \langle \sigma_{ic} \rangle = \frac{1}{2}[\sigma_{ic} + |\sigma_{ic}|] \tag{9}$$

σ_{ic}: are the principal concrete stresses

$$g^*_f = \left(\frac{\sum_{i=1}^{3} |\sigma_{ic}| R^{op}}{f((\sigma_{ij})_c)}\right)^{1+H(-r)} g_f \quad g^*_c = \left(\frac{\sum_{i=1}^{3} |\sigma_{ic}|}{f((\sigma_{ij})_c)}\right)^{1+H(-r)} g_c \tag{10}$$

$$H(-r) \begin{cases} = 0 \ if \ r > 0 \\ = 1 \ if \ r = 0 \end{cases}$$

R^{op} is the compression/tension yield threshold ratio, g_f and g_c are the maximum energy densities dissipated in uniaxial tension and compression respectively and can be evaluated as follows

$$g_f = \frac{G_f}{l_c} \text{ and } g_c = \frac{G_c}{l_c} \tag{11}$$

where G_f and G_c are fracture and crushing energies respectively and l_c is an external parameter depending on the finite element (FE) mesh that is introduced to achieve response objectivity with respect to the mesh size.

The following evolution law is used for the equivalent yield threshold,

$$K((\sigma_{ij})_c; (\kappa^p)_c) = r\sigma_t((\kappa^p)_c) + (1-r)\sigma_c((\kappa^p)_c) \tag{12}$$

where $\sigma_t((\kappa^p)_c)$ and $\sigma_c((\kappa^p)_c)$ represent the yield thresholds evolution in uniaxial tension and compression tests respectively. Exponential decay and exponential with maximum functions are used to define tension and compression hardening/softening respectively.

Loading/unloading conditions are derived from the Kuhn–Tucker relations formulated for problems with unilateral restrictions.

$$\dot{\lambda} \geqslant 0 \quad F \leqslant 0 \quad \dot{\lambda} F = 0 \tag{13}$$

4.3. Fibers constitutive model

One approximate way to represent SFRC within mixture theory is by modifying the fibers constitutive equation [42,52,53,39] according to Eq. (5). The fibers plastic deformation in conjunction with the inelastic slipping mechanism are modeled using an orthotropic elastoplastic model. Normally, fibers slip before yielding. The elastic threshold actually represents the slipping threshold. This threshold is markedly lower in fibers direction. Slipping and plastic strains are oriented in fibers direction.

To take into account this orthotropy without defining orthotropic criteria for slipping threshold, the space mapping approach is used [54,40]. This approach assumes that there are two spaces, the actual orthotropic space and the fictitious isotropic space. Stress tensors in both spaces are related through a linear transformation defined by a fourth order stress mapping tensor A_{klij} that depends on material orthotropy,

$$\tau_{kl} = A_{klij}\sigma_{ij} \tag{14}$$

where τ_{kl} y σ_{ij} are the stress tensors in fictitious isotropic space and actual orthotropic space respectively. A_{klij} is defined as a constant diagonal fourth order tensor [55],

$$A_{klij} = \delta_{im}\delta_{jn}\delta_{km}\delta_{ln}\frac{\bar{\tau}}{\bar{\sigma}_{mn}} \tag{15}$$

where δ_{im} is the Kronecker delta, $\bar{\tau}$ is the elastic threshold in the fictitious isotropic space (the same in all directions) and σ_{mn} is the value of that threshold in the actual orthotropic space in the in the direction n in the plane normal to direction m.

The problem is solved in the fictitious isotropic space and then the results are mapped to the actual orthotropic space.

A function similar to yield surface in plasticity is defined in the fictitious isotropic space to represent elastic threshold,

$$F^{ps}((\sigma_{ij})_F, (\kappa^{ps})_F) = \bar{F}((\tau_{ij})_F, (\bar{\kappa}^{ps})_F) = \bar{f}((\tau_{ij})_F) - \overline{K}((\bar{\kappa}^{ps})_F) = 0 \tag{17}$$

$\bar{F}$ is the elastic threshold function defined in the fictitious isotropic space, $\overline{K}((\bar{\kappa}^{ps})_F)$ is the hardening function and $\bar{f}$ is the equivalent stress in the fictitious isotropic space for which Von Mises function is used in this paper.

The evolution of inelastic strains in fibers and fiber/matrix interface is obtained with a flaw rule similar to the one used in plasticity theory,

$$\begin{aligned}\left(\dot{\varepsilon}^{ps}_{ij}\right)_F &= \dot{\lambda}\frac{\partial F^{ps}((\sigma_{mn})_F)}{\partial(\sigma_{ij})_F} = \dot{\lambda}\frac{\partial\bar{f}((\tau_{mn})_F)}{\partial(\sigma_{ij})_F} = \dot{\lambda}\frac{\partial\bar{f}((\tau_{mn})_F)}{\partial(\tau_{kl})_F}\frac{(\tau_{kl})_F}{\partial(\sigma_{ij})_F} \\ &= \dot{\lambda}\frac{\partial\bar{f}((\tau_{mn})_F)}{\partial(\tau_{kl})_F}A_{klij}\end{aligned} \tag{18}$$

Von Mises yield function is used as plastic potential function in the fictitious isotropic space. As a consequence of material orthotropy expressed through tensor A_{klij}, the inelastic strains are mainly oriented in fibers' direction. Force–displacement curves obtained from pull out tests are used to define inelastic hardening function $\overline{K}((\bar{\kappa}^{p}s)_F)$ in fibers direction. Inelastic work is used as hardening variable $(\bar{\kappa}^{ps})_F$ in the fictitious isotropic space.

4.4. Reinforcement model

The longitudinal and transverse reinforcement bars are not explicitly modeled as separated elements but their presence in concrete elements is taken into account using classical mixture theory explained in Section 4.1. Reinforcing steel bars are supposed to be perfectly bonded to concrete. An orthotropic elastoplastic model is used for the reinforcing bars. Orthotropy is taken into account with the space mapping approach described in Section 4.3. Von Mises yield criterion is used to define both elastic threshold and plastic potential function in the fictitious isotropic space. Due to orthotropy described by tensor A_{klij}, plastic strains are oriented in rebars direction. Force–displacement curves obtained from uniaxial tension tests are used to define plastic hardening function $\overline{K}(\bar{k}^{ps})$ in rebars' direction. Plastic work is used as hardening variable $\bar{k}^{ps}$ in the fictitious isotropic space.

5. Material mechanical properties

The models described in Section 4 were implemented in a 2D non linear static and dynamic FE program developed for research purposes. This code can be used to solve plane stress, plane strain or axial symmetric problems. Different material models are implemented in this program, particularly the plastic damage model used for concrete [41] and plasticity model used for steel rebars. Composite materials can be solved using classical mixture theory [46–48] or modified mixture theory for orthotropic materials to take into account fibers debonding and slipping. In addition to the mechanical data of all component materials and the corresponding volume proportions and orientation in case of anisotropic materials, the load displacement curve obtained from pull out tests is used as input data to characterize the hardening function corresponding to the fibers plus the fiber/matrix interface. Different alternatives to integrate constitutive equations are available but return mapping algorithm was used for all the components in this paper. Displacement control is used and non linear equilibrium equations are solved with Newton Raphson method.

First the material mechanical properties were calibrated. For this purpose, material characterization tests were numerically reproduced. The plain concrete properties are indicated in Table 4 that includes the normal strength concrete used in beams and the high strength concrete used as matrix in SFRC jacketing. Some of the properties were obtained from standard compression tests [56] and modulus tests [57]. The rest of the properties were indirectly adjusted to fit the experimental response in material characterization tests.

The FE mesh used to simulate notched beams flexure tests is shown in Fig. 2(a). A sensitivity analysis was carried out in order to choose the adequate mesh size. The mesh was refined around the notch where the inelastic process is expected to localize. A zoom of that part is also shown in Fig. 2(a). Plain stress elements were used. The dimensions of the beams are those of a notched Rilem beam [58].

From Table 4 it can be seen that high strength concrete has greater fracture energy G_f and greater ratio $R^{0p} = \sigma_{yc}/\sigma_t$ between compression yield strength σ_{yc} and tension strength σ_t, than normal strength concrete. In fact, for high strength concrete the tension strength is slightly higher than that corresponding to normal strength concrete [59].

Many normal and high strength concrete notched beams were tested. The numerical response of normal strength and high strength plain concrete beams and their comparison with average experimental results are presented in Fig. 2(a) where load versus crack mouth opening displacement (CMOD) is represented. A good correlation between numerical and experimental results is obtained for the materials parameters presented in Table 4.

For the numerical simulation of SFRC beams the amount of fibers in the axial direction was directly obtained counting the fibers approximately parallel to the beam axis going through the central section after the tests. The result of this account was quite near to 40% of the total volume of fibers that was also theoretically suggested by Torrijos [60].

The mechanical properties used to characterize the set of steel fibers and interface are presented in Table 5. Fiber pull-out tests results were used to define hardening behavior in fiber axial direc-

Table 4
Plain concrete properties.

Properties	Concrete	
	Normal strength (RC beams)	High strength (jacketing)
Elasticity modulus E (MPa)	24,010	41,500
Poisson ratio v	0.2	0.2
Uniaxial compression strength σ_{uc} (MPa)	26.3	95.3
Uniaxial compression yield threshold σ_{yc} (MPa)	18.0	67.0
Compression/tension elastic limit ratio R^{0p}	7.0	22.5
Compression equibiaxial/uniaxial ratio R^{bc}	1.16	1.16
Parameter to control the shape of yield function in the octahedral plane [41] γ	3.5	3.5
Plastic hardening variable value for the peak compression stress κ^{p}_{comp}	0.15	0.15
Fracture energy G_f (MPa mm)	0.08	0.125
Crush energy G_c (MPa mm)	6.6	10.6

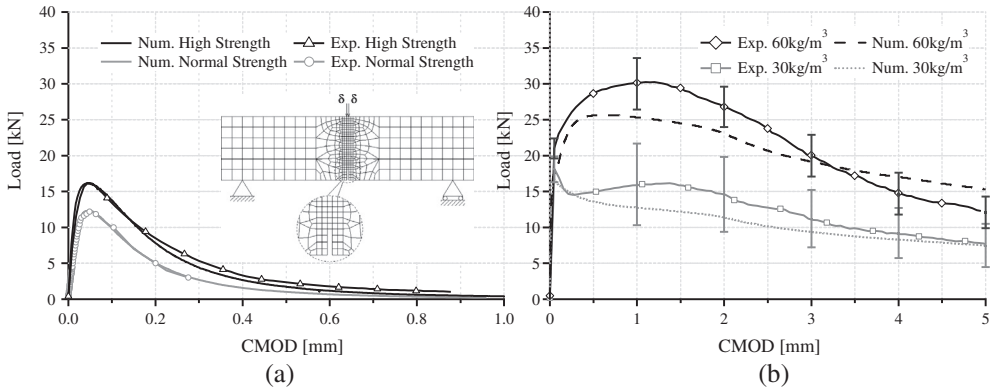

Fig. 2. Average experimental and numerical results. (a) Plain concrete beams; (b) SFRC beams.

Table 5
Properties used to model the set of fiber and interface.

Properties	
Elasticity modulus E_{xx} (MPa)	210,000
Poisson ratio $v_{xy} = v_{xz} = v_{zy} = v_{yz}$	0.2
Elasticity modulus $E_{yy} = E_{zz}$ (MPa)	1
Poisson ratio $v_{yx} = v_{zx}$	9.52e−7
Uniaxial tensile slip strength in axial direction σ_{utx} (MPa)	820.2
Uniaxial tensile slipping threshold in axial direction σ_{stx} (MPa)	29.0
Elastic threshold ratio $\sigma_{stx}/\sigma_{sty} = \sigma_{stx}/\sigma_{stz}$	0.0001

x is the axial fiber direction, y and z are normal to fiber direction.

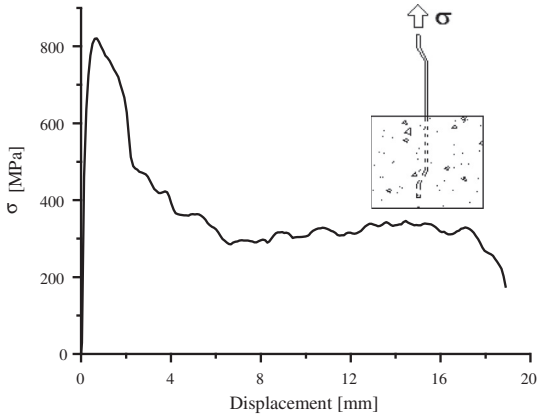

Fig. 3. Average experimental fiber pull-out response [61].

tion. A force–displacement diagram obtained from pull-out tests of steel fibers from the concrete matrix used in the SFRC jacketing [61] is presented in Fig. 3. This pull-out curve corresponds to a fiber normal to the crack face.

The comparison between numerical and average experimental results for SFRC beams bending tests for two different amounts of fibers (30 kg/m^3 and 60 kg/m^3) are presented in Fig. 2(b). While the numerical response obtained for the beams with 30 kg/m^3 of fibers approximately follows experimental response, the numerical response of the beams with 60 kg/m^3 of fibers is under the experimental average curve. However, the numerical response can reproduce the bending hardening behavior making evident the change in the mechanical response with the increase of fibers.

The scatter of experimental results for SFRC beams tests is usual for this type of material. As illustration, the standard deviation of experimental results for SFRC is also plotted on Fig. 2b. When fibers dosage is increased it is more difficult to achieve a homogeneous distribution of fibers and fibers orientation in concrete matrix. The model presented assumes very simple distributions of fibers and so it is expected to have greater differences with experimental results when fibers content is increased. The differences obtained between numerical and experimental results can the attributed to the presence of fibers slightly inclined with respect to the normal fracture plane. These fibers present higher pull-out resistance than that indicated in Fig. 3.

6. Numerical simulation of beams

This section presents the details of the numerical simulation of RC beams and the comparison with tests results. The beams were approximately modeled using the same code employed in Section 5. The strengthened beams and the whole process of testing, repairing and re-testing were simulated. A special algorithm was developed to reproduce the complete process. The numerical

model and software developed are useful for the study and design of strengthening or repairing schemes of RC structures with SFRC.

6.1. Finite element model

Fig. 4 shows the FE mesh used. The mesh looks coarse, but the problem was numerically simulated with a more refined mesh (half the element size) and similar results were obtained. Plain stress four node 50×50 mm elements with 2×2 Gauss points were used. The boundary conditions are also shown in Fig. 4; the beam was simply supported and displacement increments were applied in the third of the span. Four different colors can be distinguished from up to down, each one corresponding to a different composite material, the composition of which is indicated in Table 6 for the different beams tested. Modified mixture theory was used to model SFRC. The bottom layer is made of SFRC. The rest of the layers are assumed as composite materials made of concrete, longitudinal and transverse reinforcement and SFRC jacketing. Classical mixture theory was used to combine these materials. Each line in Table 6 corresponds to a different composite material indicated in Fig. 4 with different colors. The first three lines correspond to RC beams, while the four last lines correspond to strengthened or repaired RC concrete beams. The bottom layer indicated in white in Fig. 4 is absent in RC concrete beams. The volume percentage of the different component materials of each composite material are indicated in Table 6. For example, the first line corresponds to the concrete core of RC beams indicated as composite material number one and composed of 99.7% of concrete and 0.3% of stirrups reinforcement. The second and the third lines correspond to the bottom and upper layers and they are indicated as composite materials 2 and 3. They are both composed of concrete and longitudinal reinforcement in different percentages. For the case of strengthen or repaired RC beams composite material 1 is composed of the concrete core that includes concrete and stirrups and of the lateral jacketing which is in turn a composite material formed by concrete and fibers with different percentages depending on the material used for the jacketing (plain concrete, SFRC with 30 kg/m^3 fibers or SFRC with 60 kg/m^3 fibers). The mechanical properties of steel rebars are presented in Table 7.

6.2. Repairing algorithm

An evolutionary process was used to model the tests of the RC beams previously damaged and then repaired without changing the FE mesh. The process has two load steps. The first step corresponds to the shear load of RC beams to damage them. The second step corresponds to the shear load of repaired beams.

Fig. 5 illustrates the procedure. The FE mesh is the same in both loads steps and includes the bottom part of the jacketing.

In the first load step the behavior of the RC beam under shear is reproduced. Thus, the beam width is that of the RC beam and the volumetric fractions corresponding to the jacketing materials are set to zero. In this way the contribution of these materials to the stiffness and strength of the RC beam is null. The bottom supports are placed just under the RC bottom layer. The first load step is conducted applying vertical displacement increments in correspondence with the load point up to the maximum displacement reached in the tests. Then the RC beam is unloaded with displacement control until the vertical force is null. During this first loading step concrete and steel rebars are inellastically deformed. At the end of the first step, damage of the RC beam is represented by the values of the internal variables of concrete and reinforcement bars.

After the first load step, the width of the beam is enlarged and the volume ratios of the jacketing materials are set to their actual values to represent the addition of the jacketing. Although jacketing materials did not contribute to the response of the RC beam in the first load step, the corresponding strains, stress and internal variables resulted not null, so they are reset to null values after the first load step. In this way, at the beginning of the second load step the repaired beam is made of damaged RC plus intact SFRC. The supports are moved below the jacketing and all displacements are reset to zero since in the tests the displacements were measured from the repaired beams initial position.

The second load step is conducted like the first load step with displacement control applied on the repaired beam up to the maximum displacement reached in the test.

This algorithm was implemented in the FE code described in Section 5.

7. Numerical results

7.1. RC beams and repaired beams

7.1.1. RC beams

Like in tests performed with displacement control, the numerical simulation of RC beams under shear was performed applying quasistatic increasing vertical displacements at the load point.

The numerical response obtained for the RC beams that were later repaired with different materials and the comparison with individual tests is presented in Fig. 6 representing load versus vertical displacement of load point curves. It can be seen that the numerical simulation accurately reproduces the global stiffness and is among experimental response of beams. Nevertheless, it should be remarked that the tests of unreinforced beams showed great dispersion. The dispersion is very low for the first part of the tests but increases for displacements greater than 4 mm. The maximum coefficient of variation is 0.23 and it is comparable to those obtained by other authors for shear tests of RC beams [62] and it can be attributed to the failure mechanism.

Among researchers it is generally accepted that shear mechanism in RC structures is complex and hard to reproduce numerically. The difficulty could be attributed to the diversity of contributions present in the shear resistant mechanism, the multi-axial stress

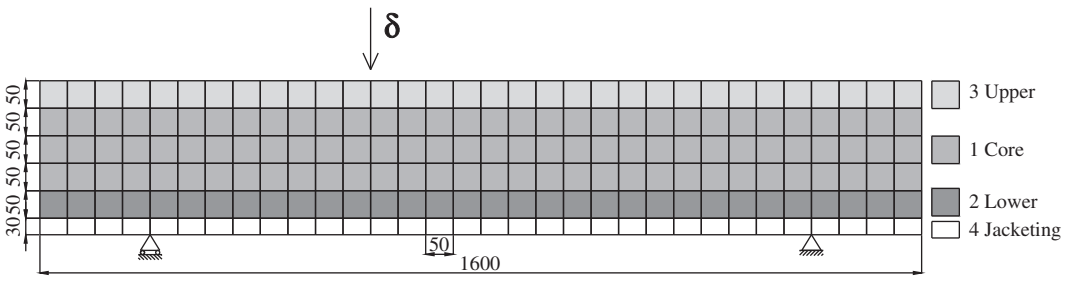

Fig. 4. Finite element mesh and materials.

Table 6
Materials volume fractions. Beams without reinforcement and strengthened/repaired beams.

Composite material				Component materials volume fraction					
Beam	Mat.N°	Concrete %	Transv. reinf. %	Long. reinf. %	Jacketing				
						Concrete %		Fiber x and y direction $k_{Fx} = k_{Fy}$%	
RC	1	99.7	0.3	0		0		0	
	2	91.7	0.3	8		0		0	
	3	98.36	0.3	1.34		0		0	
					Plain concrete	SFRC 30 kg/m^3	SFRC 60 kg/m^3	SFRC 30 kg/m^3	SFRC 60 kg/m^3
Str./Rep.	1	71.21	0.21	0	28.57	28.46	28.35	0.055	0.11
	2	65.5	0.21	5.71	28.57	28.46	28.35	0.055	0.11
	3	70.26	0.21	0.96	28.57	28.46	28.35	0.055	0.11
	4	0	0	0	1.0	99.62	99.24	0.19	0.38

state generated and the great amount of non-linearity proper of diagonal cracking of concrete [63]. It is interesting to stand out that in these beams the non linear post peak response curve is mainly defined by concrete softening behavior because steel bars have still much energy dissipation capacity at the end of the tests. The numerical simulations showed that post peak behavior of these RC beams under shear is strongly sensitive to crushing behavior of concrete. The first damage of the beams is of shear type with diagonal cracking. Finally a mechanism is formed and collapse is produced by concrete crushing near the load point.

7.1.2. Repaired beams

The numerical results for the beams previously damaged and later repaired with different materials are shown in Fig. 7 where load versus vertical deflection of the load point curves are plotted. Experimental responses of these beams are also plotted in Fig. 7 for comparison. The average experimental results of the unreinforced RC beams when they were first loaded to damage them are also included in Fig. 7.

Most of the repaired beams reached greater loads than when they were first damaged. Considering average values it can be concluded that the repair jacketing increased beams load bearing capacity and that the average strength increased with the fiber content of the SFRC jacketing.

Fig. 7(a) shows the load–displacement response of beams repaired with plain concrete. The initial stiffness and strength was recovered and even exceeded by the repaired beams due to the section enlargement. Experimental responses show great dispersion that can be attributed to brittle mechanism of jacketing debonding. Some experimental curves presented load drops caused by the jacketing debonding. The numerical response approximately reproduces the behavior of the beams repaired with plain concrete but the numerical response is closer to that of the repaired beam that did not exhibit jacketing debonding because in the numerical model the SFRC jacketing was supposed to be perfectly bonded to the beam.

The load–displacement response of beams repaired with SFRC with 30 kg/m^3 of fibers is presented in Fig. 7(b). The repaired beams exhibit very good stiffness restitution and initial strength was surpassed in all cases. The addition of fibers to the jacketing helps preventing the debonding from the beam core. The numerical response is close to the average experimental response.

The load–displacement response of beams repaired with SFRC with 60 kg/m^3 of fibers is shown in Fig. 7(c). Stiffness and load bearing capacity were substantially recovered and increased with this material. The jacketing remained perfectly bonded to the beam core due to the increase of fibers content. The beams repaired with SFRC with 60 kg/m^3 of fibers, Fig. 7(c), presented the greatest strength increase with respect to the RC beams previously tested. Nevertheless it must be noted that these results may be partly due to the fact that they were subjected to lower displacements in the previous test before they were repaired. Numerical response reasonable reproduces the load bearing capacity of the repaired beams but some differences can be observed in initial stiffness and the post-peak load that is overestimated. It should be noted that the average experimental response of the RC beams that were later repaired with SFRC with 60 kg/m^3 of fibers was more brittle than that of the rest of the RC beams, evidencing the presence of some defects in concrete causing an early crushing failure on top concrete and sudden drop of load bearing capacity. This type of behavior is also obtained for the repaired beams. The numerical model assumes the homogeneous properties for concrete and thus it is not able to capture this type of effects.

7.2. Beams strengthened with FRC

The numerical response of the strengthened beams and their comparison with average experimental results for the different types of strengthening materials are shown Fig. 8. The average experimental response of the RC concrete beams (without jacketing) is also plotted in these figures to show the effect of this strengthening technique. It can be seen that in almost all cases the strengthened beams had greater bearing capacity than the unreinforced beams and due to the jacketing, the load bearing capacity is maintained during further deformation. Comparing Fig. 8a–c, corresponding to plain concrete jacketing and SFRC with

Table 7
Reinforcement steel properties.

Properties	Long. rebars	Stirrups	Hangers
Elasticity modulus E_{xx} (MPa)	200,000	200,000	200,000
Poisson ratio $v_{xy} = v_{xz} = v_{zy} = v_{yz}$	0.2	0.2	0.2
Elasticity modulus $E_{yy} = E_{zz}$ (MPa)	100,000	20	100,000
Poisson ratio $v_{yx} = v_{zx}$	0.1	0.00002	0.1
Yield stress in x σ_x (MPa)	485	525	452
Elastic yielding threshold ratio $\sigma_{xx}/\sigma_{yy} = \sigma_{xx}/\sigma_{zz}$	0.001	0.001	0.001

x is the axial direction, y and z are normal to bar direction.

Step 1	Shear Load of RC Beams
First Load Initial Setup	
	RC beam width
	% jacketing materials null
	Supports under bottom RC layer
Load - Unload	
	Displacement increments up to maximum displacement
	Unload

Step 2	Shear Load of Repaired Beams
Repair	
	Enlarge beam width to repaired beam width
	Reset materials % to their actual value in repaired beams
	Reset jacketing materials stresses, strains and internal variables to zero
Reloading Setup	
	Reset all displacements to zero
	Move the supports to the bottom of repaired beam
Reloading	
	Displacement increments up to maximum displacement.

Fig. 5. Repairing procedure.

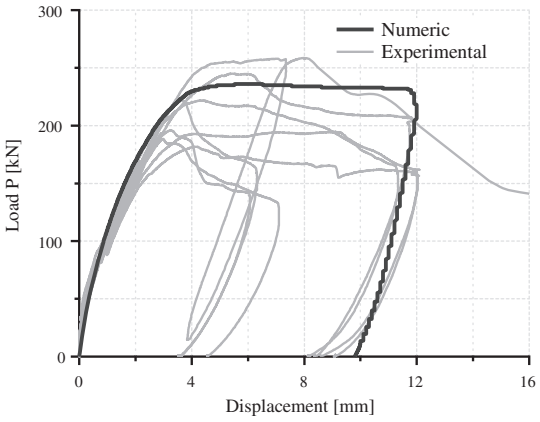

Fig. 6. RC beams numerical and experimental responses.

different fibers contains jacketing, it can be observed that the addition of fibers to the jacketing not only helps maintaining adherence with the concrete core but also contributes to the increase of load bearing capacity.

Fig. 8(a) shows the load–displacement response of beams strengthened with plain concrete. In this case, great differences were obtained in the tests for similar beams. The dispersion of experimental responses can be attributed to jacketing debonding that was evident in one beam but not in the case of the other. Since the numerical model assumes perfect bonding between the jacketing and the concrete core, the numerical response is close to that of the most resistant beam.

The load–displacement response of beams strengthened with SFRC with 30 kg/m^3 of fibers is shown in Fig. 8(b). One of the experimental curves presents abrupt load decay due to jacketing debonding. It can be seen that numerical response follows experimental results of the beam that did not exhibit jacketing debonding, slightly overestimating the peak load.

The load–displacement response of beams strengthened with SFRC with 60 kg/m^{3}of fibers is presented in Fig. 8(c). It can be seen that numerical response is close to experimental results.

8. Other strengthening/repairing alternatives

The effect of different variables of the SFRC strengthening on the shear performance of the repaired or strengthened beams is numerically studied in this section.

The response of strengthened beams with different SFRC jacketing thickness (20 mm, 30 mm and 40 mm) was numerically reproduced. The jacketing concrete matrix, the fiber type and contents were the same as in the experimental program. The responses of the strengthened beams are presented in Fig. 9. As expected, it can be seen that the load bearing capacity increases with the jacketing thickness (constant fiber content) and also increases with fiber content for constant thickness. It should be observed that stiffness and strength of strengthened beams are more sensitive to jacketing thickness than to jacketing fiber content. Nevertheless, it must be taken into account that these numerical simulations are not able to capture the fibers action preventing jacketing debonding. Experimental results show the importance of this action suggesting that fibers content should at least be enough to achieve suitable jacketing adherence to the RC beam. On the other side, there is an upper limit to fibers content given by workability of SFRC so that it can be poured in the jacketing thickness.

Jacketing thickness should be large enough to allow SFRC pouring. Upper limit to the jacketing thickness is usually given by the need of reducing additional mass of the structure and economical and aesthetic aspects.

The effect of using different strength concrete for the jacketing is also numerically analyzed. The high strength concrete used for the jacketing in the tests and a normal strength concrete, similar to that used for the RC beams, with $E = 29,500$ MPa, $\sigma_{uc} =$ 38.8 MPa, $\sigma_{fc} = 26$ MPa and $R^{0p} = 12$ are compared. The same steel fibers (normal strength fibers) and fibers contents than in the experimental tests were used in this case. The fibers pull out response not only depends on the fibers geometry and properties but also on the matrix properties. The stress–displacement curve used to define the fibers hardening for normal strength concrete is obtained from experimental pull out tests [64] and is shown in Fig. 10.

The numerical responses of the beams strengthened with SFRC using different strength concretes for the matrix are presented in Fig. 11. Different fibers contents are compared for constant jacketing thickness (30 mm). As expected, the bearing capacity of the

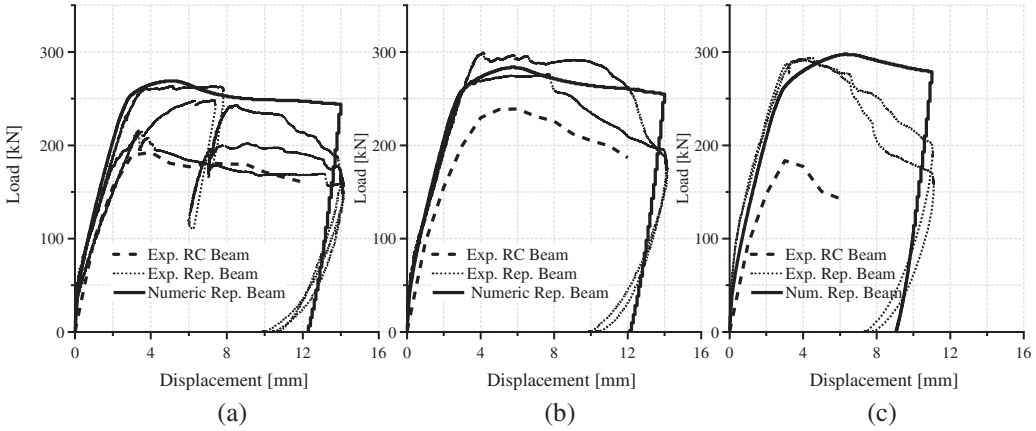

Fig. 7. Repaired beams with SFRC. (a) Plain concrete. (b) SFRC with 30 kg/m^3 of fibers. (c) SFRC with 60 kg/m^3 of fibers.

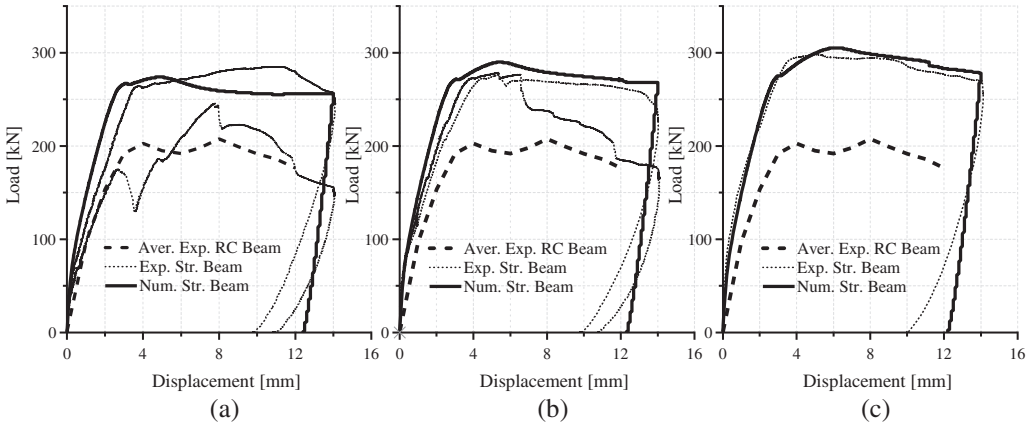

Fig. 8. Beams strengthened. (a) Plain concrete. (b) SFRC with 30 kg/m^3 of fibers. (c) SFRC with 60 kg/m^3 of fibers.

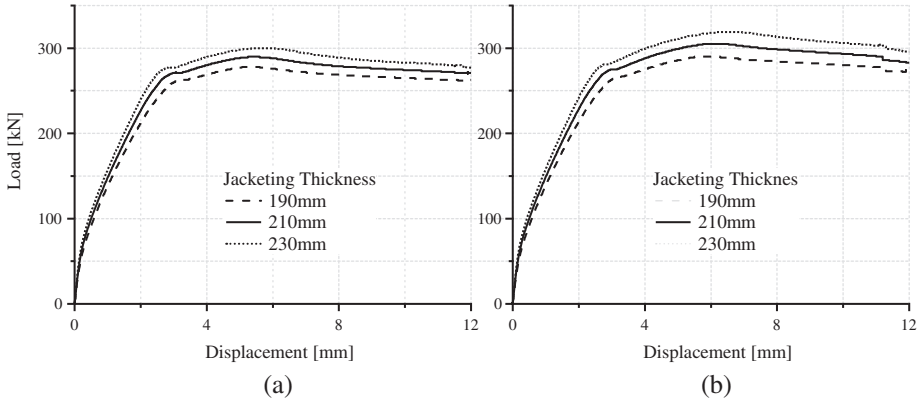

Fig. 9. Effect of jacketing thickness. (a) SFRC 30 kg/m^3 jacketing, (b) SFRC 60 kg/m^3 jacketing.

strengthened beams increases with the strength of the concrete used for the SFRC jacketing. Nevertheless, as the jacketing is very thin, the increase of load bearing capacity achieved using higher concrete strength for the jacketing is low.

The effect of using a different fiber type for the SFRC jacketing is also analyzed. Hooked end high strength fibers with *length*/*diameter* = 60 mm/0.71 mm inserted in high strength concrete matrix were considered. The corresponding pull out curve is shown in Fig. 10. The numerical response of RC beams strengthened with SFRC concrete made of the same high strength concrete but with different types of fibers are presented in Fig. 12 for comparison. The curves in each figure correspond to the same fiber content. The beams strengthened with SFRC with more resistant fibers present slightly higher post peak load bearing capacity. It should be observed that, although the pull out response of one fiber is strongly different (see Fig. 3 and solid line in Fig. 10), the effects on the

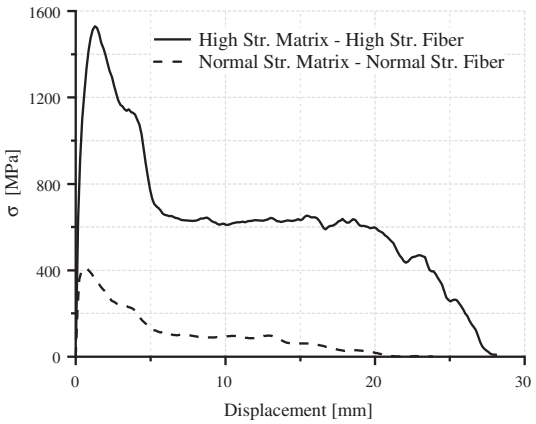

Fig. 10. Pull-out responses for normal strength fiber inserted in normal strength matrix and high strength fiber inserted in high strength matrix.

behavior of the strengthened beams are slightly different. Actually, the key value for SFRC behavior is fibers pull out strength per unity of fibers mass because equal fibers dosages are being compared. Even considering this, the results in Fig. 12 show that fibers type slightly affects the behavior of SFRC strengthened beams. This conclusion is in coincidence with that related to fibers content. Nevertheless, it should be noted again that the continuous numerical model used is not able to capture aspects related to SFRC cracking control, debonding and durability that would be essential points to choose one or other type of fibers. Experimental evidence [64,65] show that there is an optimum fiber aspect ratio. On the other side, to facilitate SFRC pouring, fiber length should be conditioned by jacketing thickness. Fibers strength should be enough to prevent fiber rupture before sliding. This aspect is not only related to fibers strength itself but also with SFRC matrix strength.

The behavior of a beam strengthened with SFRC jacketing only in the lateral sides is also studied. The numerical results obtained showed that the behavior of the strengthened beam is similar to that corresponding to the strengthened beams including the bottom SFRC reinforcing layer. Nevertheless, it should be taking into account that the bottom part helps preserving the monolithic behavior of the jacketing and hides the bottom damage face of the beam.

An additional repairing case is analyzed. The repairing of beam on both sides and at the bottom, but only on the half of the beam where the load is located (see Fig. 13) is studied. The results of this numerical simulation are very close to those including the repairing in the full length. This type of repairing represents an important save of SFRC but it would be conditioned by aesthetic reasons.

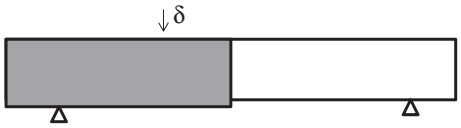

Fig. 13. Partial repairing layout.

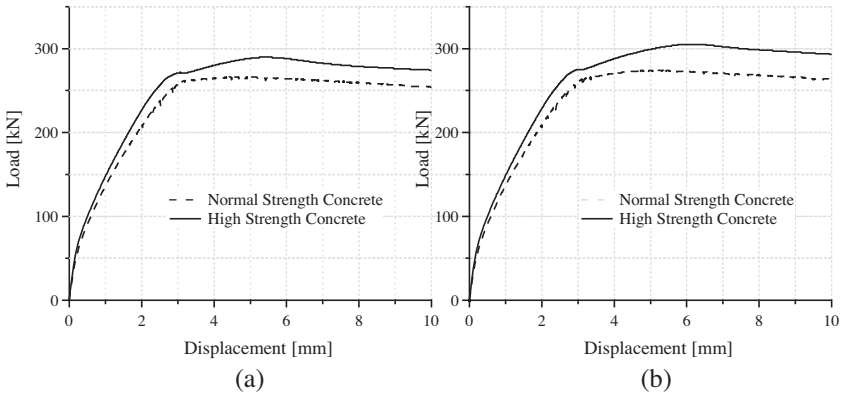

Fig. 11. Effect of jacketing concrete strength on strengthened beam behavior. (a) SFRC 30 kg/m^3 jacketing, (b) SFRC 60 kg/m^3 jacketing.

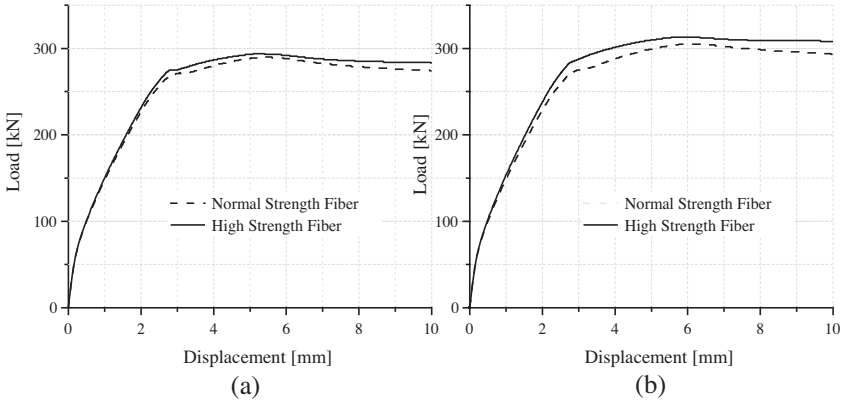

Fig. 12. Effect of type of fibers used for the SFRC jacketing on strengthened beam behavior. (a) SFRC 30 kg/m^3 jacketing, (b) SFRC 60 kg/m^3 jacketing.

9. Conclusions

A simple numerical approach to model SFRC is used to simulate the behavior of reinforced concrete beams strengthened and repaired with this material tested under shear.

The contribution of fibers to the behavior of SFRC is considered in a simple way using a modification of classical mixture theory that can be straightforward implemented in a displacement based non linear finite element program. Fibers and fibers/matrix behavior are jointly characterized with experimental fiber pull-out curves that depend not only on fibers material and geometry but also on the concrete matrix properties. The assumption of fibers orientation in three orthogonal directions is acceptable. More information about the distribution of fibers in different SFRC elements and of the percentage of fibers effectively being pull out across fissures would help to improve numerical results for SFRC. Nevertheless, taking into account the dispersion of experimental results, the numerical model used for SFRC approximately reproduces characterization tests.

The model used to simulate the RC beams, strengthened and repaired beams in two dimensions without explicitly modeling reinforcement and the jacketing, but considering them as components of a composite material, is useful to reduce computational time and gives a reasonable approximation of the whole element behavior.

The method developed to reproduce the damaging and repairing process allows keeping the changes suffered in the first loading and objectively represents its behavior in the second stage. The composite structure is well reproduced and load bearing capacity is approximately assessed.

Composite hysteretic behavior can be simulated combining elastoplastic models for the components within the composite approach presented in this paper. Only unloading curves have been simulated for the tested beams and they show a slight non-linearity. The model should be further calibrated to reproduce the shape of the hysteresis loops obtained in the tests.

The numerical model developed helps understanding the behavior of the strengthened and repaired beams and can be useful for the design of this type of intervention technique.

The following conclusions can be derived from the numerical simulations and comparison with experimental results.

Experimental results of reinforced concrete beams showed great dispersion. Numerical results obtained for these beams are close to the average experimental results. The simulations show that the post-peak response depends on concrete behavior because the steel bars still have great energy dissipation capacity. The post peak behavior of these RC beams under shear is strongly sensitive to crushing behavior of concrete because the final collapse is produced by concrete crushing near the load point.

The strengthened/repaired beams with plain concrete and fiber reinforced concrete showed greater bearing capacity than the reinforced concrete beams used for comparison and load can be further maintained in the post peak response. The simulation of strengthened beams approximately reproduce experimental results of beams that do not exhibit jacketing debonding. Both experimental and numerical results show that load bearing capacity and post peak behavior are slightly sensitive to the jacketing fiber content. Nevertheless, experimental results show that plain concrete jacketing debonding is responsible for the strengthening system failure and that the addition of fibers to the jacketing contributes to prevent its debonding from the RC concrete beam. The numerical model assumes perfect bonding between the jacketing and the RC beam and, thus it cannot simulate jacketing debonding. In order to completely assess the fiber contributions it is important to model this effect. This improvement could be done with an approach similar to that used to model fibers debonding/slipping.

For the design of this type of intervention it is important to simulate the behavior of the resulting composite structures considering all the design variables: jacketing extension and thickness, concrete mechanical properties, fibers contents and type of fibers.

Numerical simulations made with different thicknesses show that, as expected, the whole behavior does not significantly vary. Therefore, it would be advisable to define the thickness considering working conditions, price and additional mass added to the structure.

Numerical results also showed that the length of the repairing zone can be reduced to the damaged zone with practically the same results and a considerable saving of repairing material.

The improvement of concrete strength also contributes to the enhancement provided by this intervention technique but the increase in load bearing capacity is slightly sensitive to the SFRC jacketing concrete strength.

According to the numerical results presented in this paper the effect of content and type of fibers on the response of the repaired or strengthened beams with SFRC jacketing is slightly perceptible. Nevertheless, it should be noted that the continuous mechanical model used is not able to capture some important facts like workability, debonding, durability and aesthetic aspects. The selection of the content and type of fiber should be done considering the above mentioned aspects. Taking into account available experimental results, general rules can be stated. Fibers content should be enough to prevent jacketing debonding but limited to assure SFRC workability and pouring. Fibers slender should be enough to control jacketing cracking but fibers length is conditioned by the jacketing thickness. Fibers strength should be chosen in relation with concrete matrix strength to prevent fibers breakage before sliding.

Acknowledgements

The authors wish to thank the financial support of National Agency for Scientific and Technological Promotion, National Scientific and Technological Research Council (CONICET) and National University of Tucumán research Council (CIUNT) and Ms. Amelia Campos for the English revision. The companies, Tensolite S.A., Cemento Avellaneda S.A. and Maccaferri Argentina S.A. that casted and cured the beams, provided the concrete and the fibers for the experimental program, respectively, are also greatly acknowledged.

References

[1] Nanni A. A new tool for concrete and masonry repair: strengthening with fiber-reinforced cementitious matrix composites. Concr Int 2012;34(4):43–9.
[2] Naaman AE, Paramasivam P, Balazs GL, Eibl J, Erdelyi L, Hassoun NM, et al. Reinforced and prestressed concrete using HPFRCC matrices. High performance fiber reinforced cementitious composites. RILEM Proc 1996;31:291–348.
[3] Mesbah HA, Kassimi F, Yahia A, Khayat H. Flexural performance of reinforced concrete beams repaired with fiber-reinforced SCC. In: Fifth Intnl RILEM Symp on self compacting concrete; 2000.
[4] Wang YC, Lee MG. Ultra-high strength steel fiber reinforced concrete for strengthening of RC frames. J Mar Sci Technol 2007;15(3):210–8.
[5] Farhat FA, Nicolaides D, Kanellopoulos A, Karihaloo KL. High performance fibre-reinforced cementitious composite (CARDIFRC) – performance and application to retrofitting. Eng Fract Mech 2007;74:151–67.
[6] Massicotte B, Boucher-Proulx G. Seismic retrofitting of rectangular bridge piers with UHPFRC jackets. BEFIB 2008.
[7] Brühwiler E, Denarié E. Rehabilitation of concrete structures using ultra-high performance fiber reinforced concrete. In: The second international symposium on ultra high performance concrete. Kassel, Germany; 2008.
[8] Skazlic M, Bjegovic D, Serdar M. Utilization of high performance fiber-reinforced micro-concrete as a repair material. Concr Repair, Rehab Retrofit 2009;II:859–62.
[9] Boscato G, Russo S. Experimental investigation on repair of RC pavements with SFRC. Concr Repair, Rehab Retrofit 2009;II:1285–9.
[10] Martinola G, Meda A, Plizzari GA, Rinaldi Z. Strengthening and repair of RC beams with fiber reinforced concrete. Cem Concr Compos 2010;32:731–9.

[11] Maringoni S, Meda A, Mostosi S, Riva P. Strengthening of RC members by means of high performance concrete. American Concrete Institute, ACI special publication; 2012. p. 201–13 [289SP].
[12] Iskhakov I, Ribakov Y, Holschemacher K, Mueller T. High performance repairing of reinforced concrete structures. Mater Des 2013;44:216–22.
[13] Blanco A, Pujadas P, de la Fuente A, Cavalaro S, Aguado A. Application of constitutive models in European codes to RC–FRC. Constr Build Mater 2013;40:246–59.
[14] Hung CC, Li SH. Three-dimensional model for analysis of high performance fiber reinforced cement-based composites. Composites: Part B 2013;45:1441–7.
[15] Liu H, Xiang T, Zhao R. Research on non-linear structural behaviors of prestressed concrete beams made of high strength and steel fiber reinforced concretes. Constr Build Mater 2009;23:85–95.
[16] Barros J, Gettu R, Barragán B. Material nonlinear analysis of steel fiber reinforced concrete beams failing in shear. In: Sixth RILEM symposium on fibre reinforced concrete (FRC) BEFIB 2004, RILEM PRO 39; 2004. p. 711–20.
[17] Haido JH, Abu Bakar BH, Abdul-Razzak AA, Jayaprakash J, Choong KK. Simulation of dynamic response for steel fibrous concrete members using new material modeling. Constr Build Mater 2011;25:1407–18.
[18] Özcan DM, Bayraktar A, Sahin A, Haktanir T, Türker T. Experimental and finite element analysis on the steel fiber-reinforced concrete (SFRC) beams ultimate behavior. Constr Build Mater 2009;23:1064–77.
[19] Peng X, Meyer C. A continuum damage mechanics model for concrete reinforced with randomly distributed short fibers. Comput Struct 2000;78:505–15.
[20] Wang ZL, Liu YS, Shen RF. Stress–strain relationship of steel fiber-reinforced concrete under dynamic compression. Constr Build Mater 2008;22:811–9.
[21] Campione G, Mangiavillano ML. Fibrous reinforced concrete beams in flexure: experimental investigation, analytical modelling and design considerations. Eng Struct 2008;30:2970–80.
[22] Antunes J, Gettu R, Kitsutaka Y. Inverse analysis procedures for determining the tensile stress–crack opening curve of concrete. RILEM TC 187-SOC 2007:31–41.
[23] Pasa Dutra VF, Maghous S, Campos Filho A, Pacheco AR. A micromechanical approach to elastic and viscoelastic properties of fiber reinforced concrete. Cem Concr Res 2010;40:460–72.
[24] Li VC, Wang Y, Backers S. Short random fiber reinforced brittle matrix composites. J Mech Phys Solids 1991;39(5):607–25.
[25] Geng YP, Leung CKY. Micromechanics-based fem simulation of fiber-reinforced cementitious composite components. Comput Struct 1997;64(516):973–82.
[26] Naaman A, Namur G, Alwan J, Najm H. Fiber pullout and bond slip. II: experimental validation. J Struct Eng 1991;117(9):2791–800.
[27] Chanvillard G. Modeling the pullout of wire-drawn steel fibers. Cem Concr Res 1999;29:1027–37.
[28] Laranjeira F, Molins C, Aguado A. Predicting the pullout response of inclined hooked steel fibers. Cem Concr Res 2010;40:1471–87.
[29] Caggiano A, Martinelli E. A unified formulation for simulating the bond behaviour of fibres in cementitious materials. Mater Des 2012;42:204–13.
[30] Soetens T, Van Gysel A, Matthys S, Taerwe L. A semi-analytical model to predict the pull-out behaviour of inclined hooked-end steel fibres. Constr Build Mater 2013;43:253–65.
[31] Cunha VMCF, Barros JAO, Sena-Cruz JM. A finite element model with discrete embedded elements for fibre reinforced composites. Comput Struct 2012;94–95:22–33.
[32] Fang Q, Zhang J. Three-dimensional modelling of steel fiber reinforced concrete material under intense dynamic loading. Constr Build Mater 2013;44:118–32.
[33] Gal E, Kryvoruk R. Meso-scale analysis of FRC using a two-step homogenization approach. Comput Struct 2011;89:921–9.
[34] Ren X, Li J. Multi-scale based fracture and damage analysis of steel fiber reinforced concrete. Eng Fail Anal 2013. http://dx.doi.org/10.1016/j.engfailanal.
[35] Radtke FKF, Simone A, Sluys LJ. A computational model for failure analysis of fibre reinforced concrete with discrete treatment of fibres. Eng Fract Mech 2010;77:597–620.
[36] Oliver J, Mora DF, Huespe AE, Weyler R. A micromorphic model for steel fiber reinforced concrete. Int J Solids Struct 2012;49:2990–3007.
[37] Caner FC, Bazant ZP, Wendner R. Microplane model M7f for fiber reinforced concrete. Eng Fract Mech 2013;105:41–57.
[38] Brighenti R, Carpinteri A, Spagnoli A, Scorza D. Cracking behaviour of fibre-reinforced cementitious composites: a comparison between a continuous and a discrete computational approach. Eng Fract Mech 2013;103:103–14.
[39] Luccioni B, Ruano G, Isla Calderón F, Zerbino R, Giaccio G. A simple approach to model SFRC. Constr Build Mater 2012;37:111–24.
[40] Luccioni B, Oller S, Danesi R. Coupled plastic damage model. Comput Methods Appl Mech Eng 1996;129:81–9.
[41] Luccioni B, Rougier V. A plastic damage approach for confined concrete. Comput Struct 2005;83:2238–56.
[42] Luccioni B, López DE. Modelo para materiales compuestos con deslizamiento de fibras. Análisis y cálculo de estructuras de materiales compuestos Junio 2002:411–31.
[43] Ruano G, Isla F, Isas Pedraza R, Sfer D, Luccioni D. Shear retrofitting of reinforced concrete beams with steel fiber reinforced concrete. Constr Build Mater 2014;54:646–58.
[44] CIRSOC 201. Reglamento argentino para estructuras de hormigón; 2005.
[45] American Concrete Institute. ACI 318. Building code requirements for structural concrete; 2005.
[46] Truesdell C, Toupin R. The classical field theories. Handbuch der Physik 1960.
[47] Oñate E, Oller S, Botella S, Miquel J. Métodos Avanzados de Cálculo de Estructuras de Materiales Compuestos. Publication CIMNE No.11, Barcelona, Spain; 1991.
[48] Oller S, Oñate E, Miquel J, Botello S. A plastic damage constitutive model for composite materials. Int J Solids Struct 1996;33(17):2501–18.
[49] Lubliner J. On the thermodynamic foundations of non-linear mechanics. Int J Non Linear Mech 1972;7:237–54.
[50] Oller S, Oliver J, Lubliner J, Oñate E. Un modelo constitutivo de daño plástico para materiales friccionales. Parte I: variables fundamentales, funciones de fluencia y potencial. Revista Internacional de Métodos Numéricos para el Cálculo y Diseño en Ingeniería 1988;4:397–428.
[51] Rougier VC, Luccioni BM. Numerical assessment of FRP retrofitting systems for reinforced concrete elements. Eng Struct 2007;29:1664–75.
[52] Luccioni BM, López DE, Danesi RF. Bond–slip in reinforced concrete elements. J Struct Eng 2005;131(11):1690–8.
[53] Isla Calderón A, Luccioni B. Modelo para hormigones reforzados con fibras. ENIEF 2008.
[54] Betten J. Application of tensor functions to the formulation of yield criteria for anisotropic materials. Int J Plast 1988;4:29–46.
[55] Toledo M, Nallim l, Luccioni B. A micro-macromechanical approach for composite laminates. Mech Mater 2008:885–906.
[56] ASTM C 39. Test method for compressive strength of cylindrical concrete specimens. Annual book of ASTM standards. 86, Volume 04.02 concrete and aggregates [section 4 construction].
[57] ASTM C 469. Standard test method for static modulus of elasticity and Poisson's ratio of concrete in compression. Annual book of ASTM standards, volume 04.02 concrete and aggregates; 1987 [section 4 construction].
[58] Vandewalle CL. Rilem TC 162-TDF. Test and design methods for steel fibre reinforced concrete. Mater Struct 2002;35:579–82.
[59] Shah AA, Ribakov Y. Recent trends in steel fibered high-strength concrete. Mater Des 2011;32:4122–51.
[60] Torrijos MC. Mesoestructura, comportamiento mecánico y propiedades de transporte en hormigón. Tesis presentada para el grado de doctor en ingeniería 2008. Septiembre.
[61] Isla F, Isas R, Ruano G, Luccioni B. Efecto de la orientación y del confinamiento en el ensayo de extracción de fibras. XXXV Jornadas Sul Americanas de Engenharia Estrutural 2012.
[62] Claderas Bohigas A. Shear design of reinforced high-strength concrete beams. Tesis doctoral. ISBN 8468819409. Universitat Politècnica de Catalunya. Departament d'Enginyeria de la Construcció; 2002.
[63] Ferreira D, Bairán J, Marí A. Numerical simulation of shear-strengthened RC beams. Eng Struct 2013;46:359–74.
[64] Isla FA, Luccioni B, Isas Pedraza RD, Sfer D. Arrancamiento de fibra de acero en matriz de hormigon. XXXIV Jornadas sudamericanas de Ingeniería Estructural 2010. Septiembre–Octubre.
[65] Wang ZL, Wub J, Wang JG. Experimental and numerical analysis on effect of fibre aspect ratio on mechanical properties of SRFC. Constr Build Mater 2010;24:559–65.